Author Manuscript

Author Manuscript

Author Manuscript

Author Manuscript

HHS Public Access

Author manuscript

Mater Today Adv. Author manuscript; available in PMC 2023 June 13.

Published in final edited form as:

Mater Today Adv. 2023 June ; 18: . doi:10.1016/j.mtadv.2023.100378.

Resolving protein-mineral interfacial interactions during *in vitro* mineralization by atom probe tomography

Sandra D. Taylor[a,*], **Jinhui Tao**[a], **Yongsoon Shin**[a], **Garry W. Buchko**[b,c], **Alice Dohnalkova**[b], **Jack Grimm**[a,d], **Barbara J. Tarasevich**[a], **Bojana Ginovska**[a], **Wendy J. Shaw**[a], **Arun Devaraj**[a,e,**]

[a]Physical and Computational Sciences Directorate, Pacific Northwest National Laboratory, Richland, WA, 99354, USA

[b]Earth and Biological Sciences Directorate, Pacific Northwest National Laboratory, Richland, WA, 99354, USA

[c]School of Molecular Biosciences, Washington State University, Pullman, WA, 99164, USA

[d]Department of Materials Science and Engineering, University of Washington, Seattle, WA, 98195, USA

[e]Metallurgical and Materials Engineering Department, Colorado School of Mines, Golden, CO, 80401, USA

Abstract

Organic macromolecules exert remarkable control over the nucleation and growth of inorganic crystallites during (bio)mineralization, as exemplified during enamel formation where the protein amelogenin regulates the formation of hydroxyapatite (HAP). However, it is poorly understood how fundamental processes at the organic-inorganic interface, such as protein adsorption and/or incorporation into minerals, regulates nucleation and crystal growth due to technical challenges in observing and characterizing mineral-bound organics at high-resolution. Here, atom probe tomography techniques were developed and applied to characterize amelogenin-mineralized HAP particles *in vitro*, revealing distinct organic-inorganic interfacial structures and processes at the nanoscale. Specifically, visualization of amelogenin across the mineralized

This is an open access article under the CC BY-NC-ND license (http://creativecommons.org/licenses/by-nc-nd/4.0/).

*Corresponding author. sandra.taylor@pnnl.gov (S.D. Taylor). **Corresponding author. Physical and Computational Sciences Directorate, Pacific Northwest National Laboratory, Richland, WA, 99354, USA. arun.devaraj@pnnl.gov (A. Devaraj).

Credit author statement

All authors contributed to writing – review and editing. **Sandra Taylor:** Conceptualization, Methodology, Validation, Formal Analysis, Investigation, Writing – Original Draft, Visualization, Supervision; **Jinhui Tao:** Validation, Formal Analysis, Investigation, Visualization; **Yongsoon Shin:** Resources; **Alice Dohnalkova**: Validation, Formal Analysis, Investigation, Visualization; **Jack Grimm:** Investigation; **Barbara Tarasevich**: Conceptualization, Resources, Writing – Original draft, Supervision, Project Administration; **Bojana Ginovska:** Writing – Original draft, Supervision, Project Administration; **Wendy Shaw**: Conceptualization, Supervision, Project Administration, Funding acquisition; **Arun Devaraj:** Conceptualization, Methodology, Formal analysis, Writing – Original draft, Supervision, Project Administration, Funding acquisition.

Declaration of competing interest

The authors declare that they have no known competing financial interests or personal relationships that could have appeared to influence the work reported in this paper.

Appendix A. Supplementary data

Supplementary data to this article can be found online at https://doi.org/10.1016/j.mtadv.2023.100378.

Author Manuscript Author Manuscript Author Manuscript Author Manuscript

particulate demonstrates protein can become entrapped during HAP crystal aggregation and fusion. Identification of protein signatures and structural interpretations were further supported by standards analyses, i.e., defined HAP surfaces with and without amelogenin adsorbed. These findings represent a significant advance in the characterization of interfacial structures and, more so, interpretation of fundamental organic-inorganic processes and mechanisms influencing crystal growth. Ultimately, this approach can be broadly applied to inform how potentially unique and diverse organic-inorganic interactions at different stages regulates the growth and evolution of various biominerals.

Keywords

Atom probe tomography; Hydroxyapatite; Amelogenin; Nanoparticle; Biomineralization; Interface

1. Introduction

During (bio)mineralization, the nucleation and growth of inorganic crystallites is regulated by interfacial interactions with organic macromolecules. Remarkable control over the particle size, structure, morphology, aggregation, and crystallographic orientation of the mineral phase at each stage of mineralization results in biominerals, such as bone, teeth, and shells, with extraordinarily unique hierarchical structures and physicochemical properties [1–6]. As an example, during tooth enamel formation, the protein amelogenin, secreted by ameloblasts into the extracellular matrix, guides the nucleation, growth, and assembly of amorphous calcium phosphate (ACP, $Ca_xH_y(PO_4)_z{\cdot}nH_2O$ where $n \sim 3–4.5$) clusters into long, thin, ribbon-like structures which transform into hydroxyapatite (HAP, $Ca_{10}(PO_4)_6(OH)_2$) [7–9]. During later stages of mineralization, protein degradation and removal is accompanied by HAP crystals weaving together to form enamel – one of the hardest and most crack resistant biominerals in nature [2,10–12]. Conversely, cases of *amelogenesis imperfecta,* where enamel is softer, hypo- or hyper-mineralized, and/or more porous, may correlate to mineralization being inhibited by excessive protein binding caused by single amino acid mutations (e.g., inhibiting the induction time for the ACP to HAP transformation and limiting growth of specific faces), as suggested by *in vitro* studies [13–17].

The role of organics is largely inferred based on microscopic observations of the chemical, spatial, structural, morphological, and constructional evolution of the inorganic crystallites themselves *in vitro* [9,13,18–24]. However, our understanding of fundamental organic-inorganic interfacial interactions regulating nucleation and crystal growth is limited due to inherent challenges in observing and characterizing mineral-bound organics by conventional microscopy [9,18,25,26]. For instance, in the context of enamel formation, the ability to resolve adsorption processes between amelogenin nanospheres and amorphous prenucleation clusters would provide invaluable insight into particle assembly and/or transformation into HAP crystallites [5,9]. Additionally, under conditions of *amelogenesis imperfecta*, where single amino acid variants result in malformed enamel, and *in vitro* studies suggesting that variants result in excessive protein binding [13–17], it is uncertain whether amelogenin

Author Manuscript Author Manuscript Author Manuscript Author Manuscript

could be incorporated into the nascent biomineral, either occluded within individual particles as they grows or trapped between particles as they aggregate. Without the ability to directly observe the spatial distribution and association of organic macromolecules relative to inorganic phases and within complex interfacial structures (e.g., particle boundaries in aggregates), insight into these fundamental phenomena (broadly occurring across biomineralization) is mired in circumspect ambiguity.

Atom probe tomography (APT) is a mass-sensitive imaging technique capable of mapping the elemental and isotopic distributions in solids and at interfaces in three-dimensions (3D), with up to sub-nanometer resolution and parts-per-million chemical sensitivity [27,28]. Its recent applications analyzing the composition of mature biomaterials, including rodent and human tooth enamel [29–32], bone [33–35], elephant tusks, dentin [36], and chiton teeth [37] demonstrate its unique ability to characterize organic-inorganic interfaces and broadly infer processes linked to mineralization. However, mechanistic insight is limited as the provenance of these structures from *in vivo* specimens is obscured by the environmental complexity which they formed under. Application of this technique to probe crystallization *in vitro* could enable one to track specific macromolecules relative to inorganic crystallites at various stages and/or conditions during crystal growth and, in turn, unravel fundamental interactions between organics and the mineral phase and reaction sequences. However, several archetypal challenges within APT/microscopy must be overcome simultaneously, including specimen preparation of unsupported nanoparticles (i.e., not bound within a robust matrix) [38,39], aggregates, and surfaces [40–44], interpretation of complex interfaces, and reliable identification of protein signatures relative to adventitious organic ions that can also be present in these systems.

This aim of this study was to resolve fundamental interactions between protein and inorganic phases influencing crystal growth, enabled through direct observation of protein distributions within complex interfacial structures at distinct stages of growth *in vitro*. Specifically, analytical techniques exploiting APT were developed and applied to the characterization of HAP crystallites mineralized in the presence of amelogenin, as a model system and relevant to understanding HAP formed during the later stages of enamel mineralization. The resulting APT tomograms of the mineralized crystallites capture complex organic-inorganic interfacial structures arising from particle aggregation. Direct visualization of the amelogenin distribution in 3D further reveals it is localized at specific sites within aggregates of HAP particles, providing unique insight into crystal growth and particle assembly mechanisms. Systematic analysis on standards, i.e., HAP surfaces with and without amelogenin adsorbed, proved critical to the development of the analytical protocol, overcoming the above-mentioned challenges, and aiding in interpreting the unique mode by which amelogenin associates within the mineralized HAP system. This study serves as a proof-of-principle, demonstrating the utility of APT in probing crystallization *in vitro* and the ability to gain unprecedented insight into fundamental processes operating at the protein-mineral interface at the nanoscale. Ultimately, the findings and approach here can be broadly applied, revealing potentially unique and diverse organic-inorganic interactions during crystal growth and evolution across various biomineralization and organic-controlled mineralization processes.

Author Manuscript Author Manuscript Author Manuscript Author Manuscript

2. Experimental methods

2.1. In vitro experiments

Systematic analyses on model systems were conducted to develop analytical procedures for characterizing organic-inorganic interfacial structures. First, standard specimens were designed to focus on characterizing a single protein-mineral interface, i.e., micron-sized single crystals of HAP with and without native recombinant murine amelogenin (M179) adsorbed on (100) surfaces (referred to as the protein-adsorbed and control specimens, respectively; Fig. 1a). Given the ubiquity of carbon/organics on surfaces, analyses of both the control and protein-adsorbed specimens enables reliable identification of protein signatures. Additionally, the interior of the HAP microcrystal was analyzed as a supplementary control (referred to as the bulk specimen) to identify chemical signatures belonging to the mineral phase.

Following reliable identification of protein and mineral signatures with the standards, nanometer-sized HAP crystallites mineralized in the presence of amelogenin were analyzed to determine how protein associates with forming mineral phases (Fig. 1b). This specimen represents HAP in the final stages of mineralization; we focused on this stage as amelogenin interacts with a single, stable mineral phase (compared to earlier stages of mineralization where phase transformations, for instance, may complicate interpretations of protein-mineral interactions, discussed more below). In this system the organic-inorganic interfacial structures are complex and the protein distribution is unknown, e.g., amelogenin could be occluded within and/or trapped between particles. In turn, this example demonstrates the necessity for developing analytical capabilities that can resolve organic-inorganic interfacial structures and processes at the nanoscale.

The specimens were synthesized *in vitro*, selecting experimental conditions relevant to understanding mineralization processes *in vivo*. That is, the conditions for the protein-adsorbed specimens were based off previous studies [13,45], where synthetic micro-crystals were exposed to 0.25 mg/mL (0.011 mM) stock amelogenin solutions in 25 mM Tris-HCl buffer at pH 8.0. The protein concentration is within reason of that expected for *in vivo* environments; i.e., the highest amelogenin concentrations in secretory enamel are 200–300 mg/mL but decrease due to degradation by enzymes in the maturation stage [46]. More so, the surface coverage (described further in the Results) is generally consistent with expectations for *in vivo* mineralization where amelogenin is believed to adsorb onto HAP surfaces while excess protein exists in the spaces between growing crystals [47]. A pH 8.0 solution was used to keep the pH above the isoelectric point of amelogenin (~pH 6.8) [45,48]. Samples were rinsed with buffer and water to remove excess protein before their coating with metal films for APT analyses. HAP surfaces exposed to similar solution conditions but without amelogenin were prepared as the control specimen, and analyzed like the protein-adsorbed specimens.

HAP crystallites mineralized in the presence of M179 were made following protocols from previous studies [13]. In brief, a protein stock solution was formed by dissolving M179 into water at ~5 mg/mL for at least three days and the protein concentration was measured using a Nanodrop UV/visible spectrophotometer. The stock solution was diluted into water

Author Manuscript Author Manuscript Author Manuscript Author Manuscript

to give a final protein concentration of 0.20 mg/mL. Aliquots of 50 mM $CaCl_2$ and 30 mM KH_2PO_4 stock solution in water were sequentially added to give final concentrations of 2.5 mM $CaCl_2$ and 1.5 mM KH_2PO_4. The pH was adjusted to 7.8 by slowly adding KOH. The sample vial was placed into a water bath at 37 °C for seven days. The sample was removed and cooled, where excess protein removed by centrifuging and washing the particles sequentially in 0.1 M phosphate buffer, 50 mM tris/4 M urea buffer, phosphate buffer, and water three times. The samples were ultrasonicated in a water bath for 30 min and then with a probe sonicator for up to 1 min.

The solution conditions for the amelogenin-mineralized HAP were chosen to reproduce the morphology, phase, and mineralization mechanisms of primary particles like HAP crystals found in enamel *in vivo* [8,32,49]. Additionally, calcium phosphate mineralization has been studied over a range of amelogenin concentrations (0.2 mg/mL – 1 mg/mL) [20], and it was found that higher protein concentrations increased the lifetime of ACP but did not change the mineralization pathway from the initial formation of ACP before its transformation to HAP. Thus, to accelerate mineral transformation, we used the lower protein concentration of 0.20 mg/mL.

2.2. Microscopic analyses

Protein-adsorption onto HAP microcrystal surfaces (i.e., the protein-adsorbed specimen) was imaged by *in situ* atomic force microscopy (AFM), collected in tapping mode at room temperature (~23 °C) with a NanoScope 8 AFM (Digital Instruments J scanner, Bruker). Hybrid probes consisting of silicon tips on silicon nitride cantilevers (HYDRA triangular lever, k = 0.088 N/m, tip radius <10 nm, resonance frequency 75 kHz in air, Applied Nano-structures, Inc., www.appnano.com) were used for the imaging. The free amplitude was set up to 20 nm in fluid, and the signal-to-noise ratio was maintained above 10. The scanning speed was 1–2 Hz. The amplitude set point was carefully tuned to minimize the average loading force (~50 pN) for stable tracking during *in situ* imaging. Images were analyzed using Nanoscope Analysis 2.0.

The amelogenin-mineralized HAP crystals were imaged using a FEI Tecnai T-12 transmission electron microscope (TEM) with a LaB_6 filament, operating at 120 kV. Images were collected digitally with a 2 × 2K Ultrascan 1000 CCD (Gatan). A sample was prepared by diluting the sample to a concentration of 3.8 mg/mL in dialysis buffer. 5 μL of suspension was deposited onto a glow-discharged TEM grid (100 mesh copper grid coated with formvar and carbon, Electron Microscopy Sciences, Hatfield, PA) and negatively stained with NanoW (Nanoprobes). The grid was gently blotted with a filter paper and air-dried.

2.3. APT specimen preparation and analytical protocol

Unique APT specimen preparation protocols were developed considering well-known topical challenges, including the preparation of unsupported surfaces (i.e., not bound within a robust matrix like bulk biomaterials), effects from differing evaporation fields between the encapsulant and particle, peak overlaps, and the presence of voids (between the coating and particles and within the pore spaces of aggregates) [27,40,42–44]. A dual-beam focused ion beam-scanning electron microscope (FIB-SEM; Thermo Fisher Scientific Helios Nanolab

Author Manuscript Author Manuscript Author Manuscript Author Manuscript

600i) was utilized to fabricate needle-shaped APT specimens [38]. Key preparation steps are summarized here and in Fig. 2. For the standards, the HAP microcrystal surfaces were first coated with ~50 nm of Cr and ~200 nm of Ag via ion beam sputter deposition (IBSD), protecting the surfaces from subsequent ion beam exposures (Fig. 2a). Chromium was chosen as the layer adhering to HAP given past successes in analyzing oxides [38,39] while Ag was deposited to improve sample conductivity as well as build sample thickness.

Within the FIB-SEM, a rectangular region on the HAP surface was isolated for analysis, coating it with ~1 μm of Pt (via electron and ion-beam induced deposition in the SEM) to protect the surface during subsequent milling using the ion beam (Ga^+, 30 kV). Both sides were trench milled and the region was extracted using the Omniprobe micromanipulator. The liftout was rotated 90° before further sectioning and mounting onto Si microposts (Fig. 2b). The sample sections on the Si microposts were then sharpened into needles by annular milling (≤ 100 nm in diameter at the tip apex), centering the Cr-HAP interface (Fig. 2c). In this geometry, the amelogenin-HAP interface is captured along the entire tip length, enabling us to analyze the protein distribution across a larger surface area relative to conventional APT specimen preparation approaches where the interface is located at a specific depth [38]. Additionally, a conformal Cr-coating was deposited around the needle-like specimens with IBSD after sharpening (not shown in Fig. 2) to prevent delamination between layers. This preparation protocol led to a high success rate (i.e., 75%, 9 out of 12 samples yielding results) collecting between ~0.9–5.0 × 10^6 ions total per sample.

To prepare the amelogenin-mineralized HAP for APT, methods for the standards were combined with an encapsulation, cross-sectioning approach developed from previous studies using oxide nanoparticles [39]. Here, the amelogenin-mineralized HAP particles were effectively embedded within a Cr-matrix by dispersing them over a Cr-coated Si wafer and overcoating with Cr (Fig. 2d). A recent study on the preparation of HAP nanoparticles for APT analysis used a similar methodology, encapsulating the specimens in Au and/or Al by atomic layer deposition [50]. Similar to preparation of the standards, the lift-out was rotated by 90° and sections were mounted onto microposts (Fig. 2e). The sections were FIB-milled to capture the particles near the center and the apex, as determined by monitoring the needle sample in cross-section during milling (Fig. 2f), and lastly conformally coated to avoid coating delamination during APT analysis. We attempted to avoid regions with voids because the porous nature of the aggregated structures can introduce uncertainties in the reconstruction [51] and poses risk of premature failure [51–53], although these could not always be screened out during sharpening given the opacity of the sections. Additionally, due to the opacity of the encapsulated region and the resolution, the nature of the HAP particle (e.g., morphology, surfaces, etc.) could not be observed with SEM and was only realized following APT reconstruction. Nonetheless, this preparation protocol led to a high success rate (i.e., 60%, 3 out of 5 samples yielding results), particularly given the challenges associated with nanoparticulate systems [39,43,50]. The sample preparation techniques developed here for protein-adsorbed and amelogenenin-mineralized HAP specimens show considerable utility for capturing organic-inorganic interfaces by APT which could be applied across a broad range of materials and studies.

Author Manuscript Author Manuscript Author Manuscript Author Manuscript

APT measurements across the different specimens were performed using a CAMECA local electrode atom probe (LEAP) 4000 X-HR at a base temperature and pressure of 40 K and $<2 \times 10^{-11}$ Torr, respectively. Field evaporation of ions from the specimen was induced by a 355 nm wavelength picosecond laser at a pulse repetition rate of 125–200 kHz. A detection rate of 0.002–0.003 ions per pulse was maintained by varying the applied specimen voltage. Based on baseline characterization of the bulk HAP, a laser pulse energy ranging from 20 to 60 pJ was selected because it provided high data quality and a reasonable sample yield. Data were reconstructed in 3D by employing the Integrated Visualization and Analysis Software (IVAS, version 3.8.8) developed by CAMECA (Madison, WI). Detailed explanations of the APT analysis procedures are provided in the Supplementary Information (SI, Fig. S1 and S2).

3. Results and discussion

3.1. Establishing analytical protocols for interfacial analyses using standards

Systematic analyses were first conducted on the control and protein-adsorbed specimens prepared *in vitro* to establish analytical protocols for characterizing well-defined organic-inorganic interfaces by APT. For the protein-adsorbed specimen, micron-sized single crystals of HAP were synthesized and exposed to 0.25 mg/mL M179 solutions for 40 min. *In situ* AFM characterization as well as prior knowledge of the general protein topography, distribution, and adsorption-interactions aided in confirming protein adsorption onto the surface. That is, under this condition, amelogenin adsorbed onto the surface exists as a monolayer of oligomers (i.e., 24-mers) with a few secondary islands on top, as shown by *in situ* AFM imaging (Fig. 1a). These observations are consistent with those from previous studies where amelogenin was largely shown to adsorb as a monolayer of oligomers over a range of M179 concentrations (0.06 mg/mL – 0.25 mg/mL) with heights ranging from 4 to 7 nm [13,45].

3.1.1. Identifying protein signatures by mass spectral analyses—APT specimens for the control and protein-adsorbed systems, prepared using the FIB-SEM protocol described earlier (Fig. 2a–c), were analyzed by APT in laser-pulsing mode. In order to reliably reconstruct the specimen's chemical distribution in 3D as well as interfacial structures between amelogenin and HAP, ionic species must be accurately assigned to their respective mass-to-charge state (m/z) peaks in the resulting mass spectra. Given the chemically-different phases present (i.e., the Cr-coating, HAP mineral, and/or amelogenin), numerous ionic species were detected (Table 1; full mass spectra in SI, Fig. S2), complicating mass spectral analyses. However, systematic analyses on the bulk mineral, control, and protein-adsorbed specimens enabled the dominant ionic species to be determined for each phase, including amelogenin (Fig. 3).

Signatures associated with the HAP mineral phase include Ca and P ionic species, where Ca^{2+} (20–24 Da) is the dominant species as observed in the bulk as well as the control, and protein-adsorbed specimens (Table 1, Fig. 3). The Cr-coating consists of various Cr and CrO ionic species, where Cr^{2+} is the dominant species is (25–27 Da); Al species (a minor impurity introduced during IBSD) is also observed in the coating. To avoid contributions

Author Manuscript Author Manuscript Author Manuscript Author Manuscript

from potential isobaric and/or polyatomic interferences, the peak from $^{40}Ca^{2+}$ at 20 Da and $^{52}Cr^{2+}$ at 26 Da (the most abundant isotopes from each ionic species) were used to denote the HAP and Cr-phases, respectively. As shown shortly, these ions (simply referred to as the Ca and Cr species, respectively, hereafter) can be used to visualize the different phases as well as the near surface regions of the mineral in the control and protein-adsorbed specimens.

Minor organic peaks in the mass spectra were analyzed to identify protein signatures (Table 1, Fig. 3). Organic signatures are absent in the bulk mineral, as expected. In both the protein-adsorbed and control specimens, $^{12}C^{2+}$, $^{14}N^{2+}$, $^{12}C^{1+}$, and $^{14}N^{1+}$ species at 6, 7, 12, and 14 Da, respectively, were present suggesting these may potentially be from adventitious organics. In comparison, the CO^{1+} and CO_2^{1+} species at 28 and 44 Da, respectively, (collectively referred to as CO_x-species) were strongly correlated with the protein-adsorbed specimen but effectively absent in the control, i.e., the signals are over an order of magnitude higher in the protein-adsorbed specimen than the control. Our observations are consistent with previous APT analyses of bulk enamel where C^{1+}, N^{1+}, CO^{1+}, and CO_2^{1+} were also commonly detected organic species, although their source was unknown [27,33,36]. Thus, the analyses here are a strong indication that the CO_x-species are specifically associated with protein signatures.

3.1.2. Interfacial characterization and visualization—Following mass spectral analyses, the spatial location of the organic ions relative to the HAP surface could be visualized across 3D chemical reconstructions of the protein-adsorbed and control specimens, further verifying organic signatures belonging to amelogenin. That is, the APT reconstruction of the protein-adsorbed specimen captures the interface between the Cr-coating and HAP phase (Fig. 4a; denoted by isoconcentration surfaces (or iso-surfaces) of Cr and Ca, respectively), consistent with the tip geometry shown in Fig. 2c. More significantly, atomic maps visualizing organic ion distributions relative to the HAP surface (Fig. 4a inset) show CO_x species strongly associated with the mineral surface (denoted by Ca ions), consistent with amelogenin adsorption in this system. In comparison, $C^{2+,1+}$ species appear more randomly distributed. Two-dimensional (2D) concentration maps and concentration profiles of the organic species relative to the HAP surface further illustrate CO_x-species' association and local enrichment on the surface (Fig. 4b and c); i.e., ~4–5 nm thick CO_x-rich domains are highly localized and heterogeneously distributed on the surface. These observations are consistent with the adsorbed-amelogenin oligomer topography measured by AFM (Fig. 1a) and predicted from previous studies [13,45], where M179 oligomers adsorb onto the HAP surface as a monolayer with secondary islands with heights of ~4–7 nm. Hotspots of $C^{2+,1+}$ and $N^{2+,1+}$ species again are randomly distributed and not strongly associated with the surface (Fig. 4b and c), suggesting these species are likely contributions from adventitious carbon/nitrogen.

In comparison to the protein-adsorbed specimen, APT reconstruction of the control specimen shows organics are not clearly associated with the HAP surface (Fig. 5a), as expected. Atomic maps visualizing organic ion distributions relative to the HAP surface show $C^{2+,\ 1+}$ species are not strongly associated with the surface while the presence

Author Manuscript Author Manuscript Author Manuscript Author Manuscript

of CO_2^{1+} is minimal and likely from noise (Fig. 5a inset). This is further illustrated by 2D concentration maps and profiles of the organic species relative to the HAP surface (Fig. 5b and c). Hotspots of $C^{2+,\,1+}$ or $N^{2+,\,1+}$ appear randomly distributed across the volume analyzed while CO_x species are again effectively absent. Thus, through combined observations from mass spectral analyses and spatially resolving the different ionic species across the protein-adsorbed and control specimens, CO^{1+} and CO_2^{1+} species are determined to best represent amelogenin. These systematic analyses on standards demonstrates how protein signatures can be reliably and unambiguously identified, and lays the foundation for probing more complex amelogenin-mineral interfaces within the mineralized amelogenin-HAP system.

3.2. Resolving protein distributions at complex interfaces in amelogenin-mineralized HAP

The methodological and analytical protocols established on the standards were applied to analyze the protein distribution in the amelogenin-mineralized HAP specimen, where organic-inorganic interfacial structures are more complex and the nature of mineral-bound amelogenin is unknown. That is, TEM imaging shows the HAP crystals appear as thin rods ~100 × ~30 nm elongated in the *c*-direction, and are highly aggregated (Fig. 1b). The specimen is also nano-crystalline based on selected area electron diffraction. The crystal morphology is largely consistent with that observed within enamel *in vivo* [8,32,49]; one difference is that *in vivo* crystals have a higher aspect ratio because they grow by addition of amelogenin and mineral at a mineralization front where ameloblasts are located. The association of amelogenin with or within the crystallites is not distinguishable [9,18,25,26].

Specimens were prepared with the tip geometry shown in Fig. 2f and analyzed by APT, where one of the three specimens is described in detail as representative for this system (see SI for replicate analyses, Fig. S3 and S4). In general, the 3D chemical reconstructions show the mineralized phase is particulate in nature, i.e., consisting of several particles, with complex morphologies. That is, using Ca isosurfaces to visualize HAP, two distinct mineral particulates are captured in the representative specimen (Fig. 6a) – one with a “Y”-shaped morphology while the other is “F”-shaped. The two replicate specimens also contained mineral particulates with similarly unique morphologies (Fig. S3 and S4). As suggested by TEM imaging and further supported by APT analyses, these morphologies are inferred to represent aggregated HAP crystals. We speculate that the extent of aggregation may be a consequence of mineralization *in vitro*. That is, while *in vivo* mineralization occurs by mineral nucleation and oriented attachment within the protein matrix [8,32,49], HAP crystals in a 3D solution can aggregate due to inherent colloidal particle-particle interactions and orient more randomly. This may in turn lead to the variety of particle morphologies observed here.

Several surfaces and interfaces exist across the particulates. Visualization of the protein-mineral interface(s) was achieved using CO_x and Ca-species, as done for the protein-adsorbed specimen. For clarity, CO_2^{1+} is used to visualize the amelogenin distribution relative to the HAP phase, as it was the more dominant organic ion; it also appears to remain strongly correlated to CO^{1+} species. In turn, it is shown that amelogenin is heterogeneously distributed across the particulates at the nanoscale, often localized within distinct regions of

Author Manuscript Author Manuscript Author Manuscript Author Manuscript

the particulates. That is, as illustrated in Fig. 6a, amelogenin is highly concentrated at the junction of the Y-particulate whereas the F-particulate has little to no amelogenin associated with it. Protein adsorption onto the outer-exposed surfaces of the particulates was seldom observed, likely due to the washing step used to remove excess protein. Similar observations were made for a mineral particulate in a separate reconstruction, with amelogenin again strongly associated with a junction (Fig. S3). Further, a subtle but interesting observation is that amelogenin is captured both above and within the junction of the Y-particulate, as highlighted by cross-sectional analysis and concentration measurements across these regions (Fig. 6b and c). Above the junction, amelogenin can be inferred to be trapped between HAP crystals while amelogenin within the junction raises the question as to whether it is trapped between or occluded within crystals of the mineral particulate.

To more clearly determine the mode by which amelogenin is associated within the aggregates, we utilized 3D visualizations of the protein distribution relative to the HAP particulate (Fig. 7a–c) coupled with cross-sectional analyses along various directions and depths (Fig. 7d and e). This enabled us to infer particle boundaries as well as the particulate's spatial evolution. These analyses in turn reveal that amelogenin localized at and above the junction of the Y-particulate is trapped between HAP crystals. That is, the particulate appears to be composed of at least three separate crystals that make contact at the junction and fuse together towards the particulate base; e.g., two crystals (denoted C1 and C2) join at the junction based on cross-sectional analyses along the x- and z-directions (Fig. 7d and e).

This is the first-time amelogenin trapped within these aggregated structures has been directly observed, enabling us to infer the interaction between amelogenin with HAP crystals at a particular stage in growth. That is, it appears HAP crystal aggregation and fusion are occurring at this stage of growth, where amelogenin, likely pre-adsorbed onto the crystals, can become trapped between crystallites. Protein above the junction is also clearly trapped between individual crystals despite incomplete fusion. We speculate amelogenin trapped in interparticle regions may inhibit crystallites from merging properly at lattice sites. Concentration measurements across this region also shows CO_x ions to be localized between two Ca-rich HAP crystals (Fig. 6c). These observations are consistent with those for another amelogenin-mineralized HAP specimen, where at least two crystals appear to fuse at a junction and trap protein in an interparticle region (Fig. S3).

The ability to directly resolve protein distributions within complex interfacial structures *in vitro* provides fundamental insight into protein-mineral interactions at distinct stages of crystal growth, where, for instance, here we capture the trapping of amelogenin between particles during fusion. Observation of these fundamental phenomena, broadly speculated to occur across bio-mineralization, have otherwise been elusive due to technical challenges in resolving complex organic-inorganic interfacial structures at high-resolution [25,26]. For future studies this approach can be applied to probe the effect of amelogenin *vs.* variants on mineralization to gain further insight into potential mechanisms regulating enamel formation. For instance, the substitution of amino acids can result in amelogenin with higher binding affinity to each other (self-assembly) and/or to HAP [13]. This may facilitate the incorporation of amelogenin into the mineral phase and, ultimately, alter the mechanical

Author Manuscript Author Manuscript Author Manuscript Author Manuscript

properties of the resulting enamel [54–58]. Thus, it would be interesting to observe whether differences exist in the association and distribution of these variants on the mineral, and what effect this may have on crystal growth.

This approach could be extended as well as combined with future technical developments to understand organic-inorganic interfacial processes and structures occurring at different stages of mineralization. In particular, studies probing the earlier stages of mineralization, where amelogenin is interacting with ACP and/or dynamic mineral phase transformations can occur [7–9], may benefit from the development of cryo-transfer and specimen preparation techniques, e.g., to preserve the nature of the meta-stable phases and/or interfacial processes in solution. As mentioned above, we intentionally focused on amelogenin interactions with HAP due to its stability and in turn did not require special environmental or cryogenic transfer tools. While cryo-techniques are still largely in the development stages for APT and are non-trivial [59], various aspects of our approach would remain applicable to deducing organic-inorganic interfacial interactions across the different stages of mineralization, such as the outlined systematic analyses for determining protein and mineral signatures as well as the cross-sectional analyses for inferring aggregation. These studies would provide invaluable insight into the fundamental role(s) of amelogenin during mineral evolution. Additionally, while not the focus of this paper, this approach could be used to probe the concurrent effect of counter ions during mineralization, as these are commonly observed in *in vivo* bulk enamel specimens though their provenance is unknown [32]. In general, this study serves as a foundation for resolving fundamental processes operating at organic-inorganic interfaces, broadly applicable to biomineralization.

4. Conclusions

Here, we demonstrate the ability to capture protein-mineral interactions and interfacial processes at the nanoscale during crystal growth *in vitro*, enabled by 3D APT. Our findings provide fundamental insight into the association of protein with mineral phases, e.g., amelogenin adsorbed onto surfaces vs. trapped between aggregated particles, of relevance to different stages of biomineralization. Systematic analyses of standards, i.e., well-defined HAP crystal surfaces with and without amelogenin adsorbed, were critical for technique development as well as interpretation of (complex) interfacial structures. Amelogenin was identified through unique mass-spectral signatures as well as by spatially resolving its distribution on a protein-adsorbed surface. The oligomer-topography was also nominally consistent with that determined by *in situ* AFM characterization. The chemical signatures extracted from the protein-adsorbed system, specifically CO_x, were used to interpret the protein distribution within complex interfacial structures of amelogenin-mineralized HAP. The protein distribution clearly differs from simple adsorption as CO_x-species are not densely localized on outer-exposed surfaces but are rather distinctly localized at particulate junctions. In turn, 3D chemical visualization and cross-sectional analyses by APT reveal that HAP crystal aggregation and fusion could lead to the incorporation of protein within interparticle regions.

Though speculated to occur broadly across biomineralization and mineralization, insight into these fundamental phenomena has been limited due to technical challenges in resolving

Author Manuscript Author Manuscript Author Manuscript Author Manuscript

complex organic-inorganic interfacial structures at high-resolution [25,26]. This study represents a significant advance in the characterization and interpretation of these structures, demonstrating that distinct protein-mineral interactions and reaction sequences during crystal growth can be resolved through *in vitro* analyses. With this proof-of-principle, we aim to extend these characterizations to systematically study hydroxyapatite mineralization by amelogenin under various conditions and at various stages of growth [54–58]. For instance, as speculated earlier for cases of *amelogenesis imperfecta* [13–17], it would be of interest to determine whether interfacial interactions and processes are characteristically different with variants, where perhaps excessive protein binding may suggest it has a higher propensity to be occluded within a particle as it grows or trapped between particles as they aggregate.

While discussed in the context of enamel formation, the approach and concepts from this study are broadly applicable to understanding the role of organic macromolecules, or more generally additives, in biomineralization and crystal growth processes [3,5,6]. Additionally, cross-sectional analyses coupled with 3D visualization has the potential to unravel complex aggregate structures which can in turn be used to deduce mesoscale-assembly and particle-based crystallization mechanisms *in vitro* or *ex situ* [60]. While each system will present new challenges regarding specimen preparation or analytical protocol, it is possible these can be overcome through benchmark studies and systematic analyses, as demonstrated here. This fundamental-level of understanding of crystal nucleation and growth mechanisms of biominerals could also ultimately aid in informing, predicting, and eventually manipulating biomaterial formation to incorporate unique physio-chemical properties into novel materials.

Supplementary Material

Refer to Web version on PubMed Central for supplementary material.

Acknowledgements

This work was supported by funding from NIH-NIDCR Grant number DE-015347. Sample preparation and measurements with APT (Cameca LEAP 4000XHR) were performed on project awards (10.46936/cpcy.proj.2019.51215/60006746) from the Environmental Molecular Sciences Laboratory, a DOE Office of Science User Facility sponsored by the Biological and Environmental Research program under Contract No. DE-AC05-76RL01830.

Data availability

Data will be made available on request.

References

[1]. Weiner S, Wagner HD, The material bone: structure-mechanical function relations, Annu. Rev. Mater. Sci 28 (1998) 271–298, 10.1146/annurev.matsci.28.1.271.

[2]. Palmer LC, Newcomb CJ, Kaltz SR, Spoerke ED, Stupp SI, Biomimetic systems for hydroxyapatite mineralization inspired by bone and enamel, Chem. Rev 108 (2008) 4754–4783, 10.1021/cr8004422. [PubMed: 19006400]

[3]. Lowenstam HA, Weiner S, On Biomineralization, Oxford University Press, New York, NY, 1989.

Author Manuscript Author Manuscript Author Manuscript Author Manuscript

[4]. Evans JS, Tuning in to mollusk shell nacre- and prismatic-associated protein terminal sequences: implications for biomineralization and the construction of high performance inorganic organic composites, Chem. Rev 108 (2008) 4455–4462, 10.1021/cr078251e. [PubMed: 18793025]

[5]. Gower LB, Biomimetic model systems for investigating the amorphous precursor pathway and its role in biomineralization, Chem. Rev 108 (2008) 4551–4627, 10.1021/cr800443h. [PubMed: 19006398]

[6]. Mann S, Archibald DD, Didymus JM, Douglas T, Heywood BR, Meldrum FC, Reeves NJ, Crystallization at inorganic-organic interfaces -biominerals and biomimetic synthesis, Science 261 (1993) 1286–1292, 10.1126/science.261.5126.1286. [PubMed: 17731856]

[7]. Fincham AG, Moradian-Oldak J, Diekwisch TG, Lyaruu DM, Wright JT, Bringas P Jr., Slavkin HC, Evidence for amelogenin "nanospheres" as functional components of secretory-stage enamel matrix, J. Struct. Biol 115 (1995) 50, 10.1006/jsbi.1995.1029. [PubMed: 7577231]

[8]. Beniash E, Metzler RA, Lam RSK, Gilbert PUPA, Transient amorphous calcium phosphate in forming enamel, J. Struct. Biol 166 (2009) 133–143, 10.1016/J.Jsb.2009.02.001. [PubMed: 19217943]

[9]. Fang PA, Conway JF, Margolis HC, Simmer JP, Beniash E, Hierarchical self-assembly of amelogenin and the regulation of biomineralization at the nanoscale, Proc. Natl. Acad. Sci. U. S. A 108 (2011) 14097–14102, 10.1073/pnas.1106228108. [PubMed: 21825148]

[10]. Robinson C, Kirkham J, Shore R, Dental Enamel: Formation to Destruction, CRC Press, 1995.

[11]. Fincham AG, Moradian-Oldak J, Simmer JP, The structural biology of the developing dental enamel matrix, J. Struct. Biol 126 (1999) 270, 10.1006/jsbi.1999.4130. [PubMed: 10441532]

[12]. Bartlett JD, Dental Enamel Development: Proteinases and Their Enamel Matrix Substrates, vol. 2013, ISRN dentistry, 2013, 684607, 10.1155/2013/684607.

[13]. Tao J, Shin Y, Jayasinha R, Buchko GW, Burton SD, Dohnalkova AC, Wang Z, Shaw WJ, Tarasevich BJ, The energetic basis for hydroxyapatite mineralization by amelogenin variants provides insights into the origin of amelogenesis imperfecta, Proc. Natl. Acad. Sci. U.S.A 116 (2019) 13867–13872, 10.1073/pnas.1815654116. [PubMed: 31239344]

[14]. Ravassipour DB, Hart PS, Hart TC, Ritter AV, Yamauchi M, Gibson C, Wright JT, Unique enamel phenotype associated with amelogenin gene (AMELX) codon 41 point mutation, J. Dent. Res 79 (2000) 1476–1481, 10.1177/00220345000790070801. [PubMed: 11005731]

[15]. Qing P, Li Y, Gao S, Qiao M, Qian L, Yu H, Characterization of the nano-scratch, microstructure, and composition in hypoplastic amelogenesis imperfecta, Adv. Mech. Eng 7 (2015), 1687814015595597, 10.1177/1687814015595597.

[16]. Wright JT, Hart PS, Aldred MJ, Seow K, Crawford PJ, Hong SP, Gibson CW, Hart TC, Relationship of phenotype and genotype in X-linked amelogenesis imperfecta, Connect. Tissue Res 44 (Suppl 1) (2003) 72–78, 10.1080/03008200390152124. [PubMed: 12952177]

[17]. Chaudhary M, Dixit S, Singh A, Kunte S, Amelogenesis imperfecta: report of a case and review of literature, J. Oral Maxillofac. Pathol 13 (2009) 70–77, 10.4103/0973-029x.57673. [PubMed: 21887005]

[18]. Bai YS, Yu ZL, Ackerman L, Zhang Y, Bonde J, Li W, Cheng YF, Habelitz S, Protein nanoribbons template enamel mineralization, Proc. Natl. Acad. Sci. U.S.A 117 (2020) 19201–19208, 10.1073/pnas.2007838117. [PubMed: 32737162]

[19]. Moradian-Oldak J, Protein-mediated enamel mineralization, FBL 17 (2012) 1996–2023, 10.2741/4034. [PubMed: 22652761]

[20]. Kwak SY, Yamakoshi Y, Simmer JP, Margolis HC, MMP20 proteolysis of native amelogenin regulates mineralization in vitro, J. Dent. Res 95 (2016) 1511–1517, 10.1177/0022034516662814. [PubMed: 27558264]

[21]. Moradian-Oldak J, George A, Biomineralization of enamel and dentin mediated by matrix proteins, J. Dent. Res 100 (2021) 1020–1029, 10.1177/00220345211018405. [PubMed: 34151644]

[22]. Shao C, Bapat RA, Su J, Moradian-Oldak J, Regulation of hydroxyapatite nucleation in vitro through ameloblasticeamelogenin interactions, ACS Biomatl Sci & Eng (2022), 10.1021/acsbiomaterials.1c01113.

Author Manuscript Author Manuscript Author Manuscript Author Manuscript

[23]. Shaw WJ, Tarasevich BJ, Buchko GW, Arachchige RMJ, Burton SD, Controls of nature: secondary, tertiary, and quaternary structure of the enamel protein amelogenin in solution and on hydroxyapatite, J. Struct. Biol 212 (2020), 107630, 10.1016/j.jsb.2020.107630. [PubMed: 32979496]

[24]. Akkineni S, Zhu C, Chen J, Song M, Hoff SE, Bonde J, Tao J, Heinz H, Habelitz S, Yoreo JJD, Amyloid-like amelogenin nanoribbons template mineralization via a low-energy interface of ion binding sites, Proc. Natl. Acad. Sci. USA 119 (2022), e2106965119, 10.1073/pnas.2106965119. [PubMed: 35522709]

[25]. Goode AE, Porter AE, Kłosowski MM, Ryan MP, Heutz S, McComb DW, Analytical transmission electron microscopy at organic interfaces, Curr. Opin. Solid State Mater. Sci 21 (2017) 55–67, 10.1016/j.cossms.2016.02.005.

[26]. Hendley CT, Tao J, Kunitake JAMR, De Yoreo JJ, Estroff LA, Microscopy techniques for investigating the control of organic constituents on biomineralization, MRS Bull. 40 (2015) 480–489, 10.1557/mrs.2015.98. [PubMed: 27358507]

[27]. Devaraj A, Perea DE, Liu J, Gordon L, Prosa TJ, Parikh P, Diercks DR, Meher S, Kolli RP, Meng YS, Thevuthasan S, Three-dimensional nanoscale characterization of materials by atom probe tomography, Int. Mater. Rev 63 (2018) 68–101, 10.1080/09506608.2016.1270728.

[28]. Gault B, Chiaramonti A, Cojocaru-Mirédin O, Stender P, Dubosq R, Freysoldt C, Makineni SK, Li T, Moody M, Cairney JM, Atom probe tomography, Nature Reviews Methods Primers 1 (2021) 51, 10.1038/s43586-021-00047-w.

[29]. Gordon LM, Cohen MJ, MacRenaris KW, Pasteris JD, Seda T, Joester D, Amorphous intergranular phases control the properties of rodent tooth enamel, Science 347 (2015) 746–750, 10.1126/science.1258950. [PubMed: 25678658]

[30]. La Fontaine A, Zavgorodniy A, Liu H, Zheng R, Swain M, Cairney J, Atomic-scale compositional mapping reveals Mg-rich amorphous calcium phosphate in human dental enamel, Sci. Adv 2 (2016), 10.1126/sciadv.1601145.

[31]. Gordon LM, Joester D, Mapping residual organics and carbonate at grain boundaries and the amorphous interphase in mouse incisor enamel, Front. Physiol 6 (2015), 10.3389/fphys.2015.00057.

[32]. DeRocher KA, Smeets PJM, Goodge BH, Zachman MJ, Balachandran PV, Stegbauer L, Cohen MJ, Gordon LM, Rondinelli JM, Kourkoutis LF, Joester D, Chemical gradients in human enamel crystallites, Nature 583 (2020) 66–71, 10.1038/s41586-020-2433-3. [PubMed: 32612224]

[33]. Langelier B, Wang X, Grandfield K, Atomic scale chemical tomography of human bone, Sci. Rep 7 (2017), 39958, 10.1038/srep39958. [PubMed: 28054636]

[34]. Lee BEJ, Langelier B, Grandfield K, Visualization of CollageneMineral Arrangement Using Atom Probe Tomography, bioRxiv, 2020, p. 2020, 10.1101/2020.07.10.197673, 2007.2010.197673.

[35]. Sundell G, Dahlin C, Andersson M, Thuvander M, The bone-implant interface of dental implants in humans on the atomic scale, Acta Biomater. 48 (2017) 445–450, 10.1016/j.actbio.2016.11.044. [PubMed: 27872014]

[36]. Gordon LM, Tran L, Joester D, Atom probe tomography of apatites and bone-type mineralized tissues, ACS Nano 6 (2012) 10667–10675, 10.1021/nn3049957. [PubMed: 23176319]

[37]. Gordon LM, Joester D, Nanoscale chemical tomography of buried organiceinorganic interfaces in the chiton tooth, Nature 469 (2011) 194, 10.1038/nature09686. [PubMed: 21228873]

[38]. Taylor SD, Liu J, Arey BW, Schreiber DK, Perea DE, Rosso KM, Resolving iron(II) sorption and oxidative growth on hematite (001) using atom probe tomography, J. Phys. Chem. C 122 (2018) 3903–3914, 10.1021/acs.jpcc.7b11989.

[39]. Taylor SD, Liu J, Zhang X, Arey BW, Kovarik L, Schreiber DK, Perea DE, Rosso KM, Visualizing the iron atom exchange front in the Fe(II)-catalyzed recrystallization of goethite by atom probe tomography, Proc. Natl. Acad. Sci. U.S.A 116 (2019) 2866–2874, 10.1073/pnas.1816620116. [PubMed: 30733289]

[40]. Devaraj A, Gu M, Colby R, Yan P, Wang CM, Zheng JM, Xiao J, Genc A, Zhang JG, Belharouak I, Wang D, Amine K, Thevuthasan S, Visualizing nanoscale 3D compositional

Author Manuscript Author Manuscript Author Manuscript Author Manuscript

fluctuation of lithium in advanced lithium-ion battery cathodes, Nat. Commun 6 (2015) 8014, 10.1038/ncomms9014. [PubMed: 26272722]

[41]. Devaraj A, Perea DE, Liu J, Gordon LM, Prosa TJ, Parikh P, Diercks DR, Meher S, Kolli RP, Meng YS, Thevuthasan S, Three-dimensional nanoscale characterisation of materials by atom probe tomography, Int. Mater. Rev 63 (2018) 68–101, 10.1080/09506608.2016.1270728.

[42]. Lewis JB, Floss C, Isheim D, Daulton TL, Seidman DN, Ogliore R, Origins of meteoritic nanodiamonds investigated by coordinated atom-probe tomography and transmission electron microscopy studies, Meteoritics Planet Sci. 55 (2020) 1382–1403, 10.1111/maps.13373.

[43]. Lewis JB, Isheim D, Floss C, Seidman DN, Distinguishing meteoritic nanodiamonds from disordered carbon Using atom-probe tomography, Microscopy Today 26 (2018) 18–23, 10.1017/S1551929518000226.

[44]. Mukherjee S, Watanabe H, Isheim D, Seidman DN, Moutanabbir O, Laser-assisted field evaporation and three-dimensional atom-by-atom mapping of diamond isotopic homojunctions, Nano Lett. 16 (2016) 1335–1344, 10.1021/acs.nanolett.5b04728. [PubMed: 26741402]

[45]. Tao J, Buchko GW, Shaw WJ, De Yoreo JJ, Tarasevich BJ, Sequence-defined energetic shifts control the disassembly kinetics and microstructure of amelogenin adsorbed onto hydroxyapatite (100), Langmuir 31 (2015) 10451–10460, 10.1021/acs.langmuir.5b02549. [PubMed: 26381243]

[46]. Robinson C, Kirkham J, Hallsworth A, Volume distribution and concentration of protein, mineral and water in developing bovine enamel, Arch. Oral Biol 33 (1988) 159–162, 10.1016/0003-9969(88)90040-4. [PubMed: 3178535]

[47]. Zhu L, Liu H, Witkowska HE, Huang Y, Tanimoto K, Li W, Preferential and selective degradation and removal of amelogenin adsorbed on hydroxyapatites by MMP20 and KLK4 in vitro, Front. Physiol 5 (2014) 268, 10.3389/fphys.2014.00268. [PubMed: 25104939]

[48]. Uskoković V, Castiglione Z, Cubas P, Zhu L, Li W, Habelitz S, Zeta-potential and particle size analysis of human amelogenins, J. Dent. Res 89 (2010) 149–153, 10.1177/0022034509354455. [PubMed: 20040742]

[49]. Beniash E, Stifler CA, Sun C-Y, Jung GS, Qin Z, Buehler MJ, Gilbert PU, The hidden structure of human enamel, Nat. Commun 10 (2019) 4383 10.1038/s41467-019-12185-7. [PubMed: 31558712]

[50]. Mosiman DS, Chen Y-S, Yang L, Hawkett B, Ringer SP, Mariñas BJ, Cairney JM, Atom probe tomography of encapsulated hydroxyapatite nanoparticles, Small Methods 5 (2021), 2000692, 10.1002/smtd.202000692.

[51]. Miller MK, Hetherington MG, Local magnification effects in the atom probe, Surf. Sci 246 (1991) 442–449, 10.1016/0039-6028(91)90449-3.

[52]. Devaraj A, Colby R, Vurpillot F, Thevuthasan S, Understanding atom probe tomography of oxide-supported metal nanoparticles by correlation with atomic-resolution electron microscopy and field evaporation simulation, J. Phys. Chem. Lett 5 (2014) 1361–1367, 10.1021/jz500259c. [PubMed: 26269980]

[53]. Devaraj A, Vijayakumar M, Bao J, Guo MF, Derewinski MA, Xu Z, Gray MJ, Prodinger S, Ramasamy KK, Discerning the location and nature of coke deposition from surface to bulk of spent zeolite catalysts, Sci. Rep 6 (2016), 37586, 10.1038/srep37586. [PubMed: 27876869]

[54]. Rae Cho K, Kim Y-Y, Yang P, Cai W, Pan H, Kulak AN, Lau JL, Kulshreshtha P, Armes SP, Meldrum FC, De Yoreo JJ, Direct observation of mineraleorganic composite formation reveals occlusion mechanism, Nat. Commun 7 (2016), 10187, 10.1038/ncomms10187. [PubMed: 26732046]

[55]. Kim Y-Y, Carloni JD, Demarchi B, Sparks D, Reid DG, Kunitake Miki E., Tang CC, Duer MJ, Freeman CL, Pokroy B, Penkman K, Harding JH, Estroff LA, Baker SP, Meldrum FC, Tuning hardness in calcite by incorporation of amino acids, Nat. Mater 15 (2016) 903–910, 10.1038/nmat4631. [PubMed: 27135858]

[56]. Kim Y-Y, Ganesan K, Yang P, Kulak AN, Borukhin S, Pechook S, Ribeiro L, Kröger R, Eichhorn SJ, Armes SP, Pokroy B, Meldrum FC, An artificial biomineral formed by incorporation of copolymer micelles in calcite crystals, Nat. Mater 10 (2011) 890–896, 10.1038/nmat3103. [PubMed: 21892179]

Author Manuscript Author Manuscript Author Manuscript Author Manuscript

[57]. Hendley CT, Fielding LA, Jones ER, Ryan AJ, Armes SP, Estroff LA, Mechanistic insights into diblock copolymer nanoparticleecrystal Interactions revealed via in situ atomic force microscopy, J. Am. Chem. Soc 140 (2018) 7936–7945, 10.1021/jacs.8b03828. [PubMed: 29916709]

[58]. Borukhin S, Bloch L, Radlauer T, Hill AH, Fitch AN, Pokroy B, Screening the incorporation of amino acids into an inorganic crystalline host: the case of calcite, Adv. Funct. Mater 22 (2012) 4216–4224, 10.1002/adfm.201201079.

[59]. McCarroll IE, Bagot PAJ, Devaraj A, Perea DE, Cairney JM, New frontiers in atom probe tomography: a review of research enabled by cryo and/or vacuum transfer systems, Materials Today Advances 7 (2020), 100090, 10.1016/j.mtadv.2020.100090. [PubMed: 33103106]

[60]. Yoreo JJD, Gilbert PUPA, Sommerdijk NAJM, Penn RL, Whitelam S, Joester D, Zhang H, Rimer JD, Navrotsky A, Banfield JF, Wallace AF, Michel FM, Meldrum FC, Cölfen H, Dove PM, Crystallization by particle attachment in synthetic, biogenic, and geologic environments, Science 349 (2015) aaa6760, 10.1126/science.aaa6760. [PubMed: 26228157]

Author Manuscript Author Manuscript Author Manuscript Author Manuscript

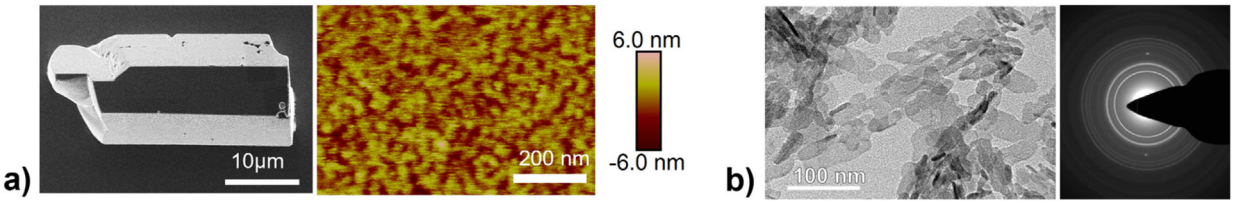

Fig. 1.

Specimens systematically analyzed. (a) SEM image of the protein-adsorbed specimen highlighting the general HAP microcrystal morphology. Amelogenin adsorption onto the crystal surface observed by high-resolution *in situ* AFM imaging. (b) TEM image of the amelogenin-mineralized HAP crystallites and electron diffraction ring pattern.

Author Manuscript Author Manuscript Author Manuscript Author Manuscript

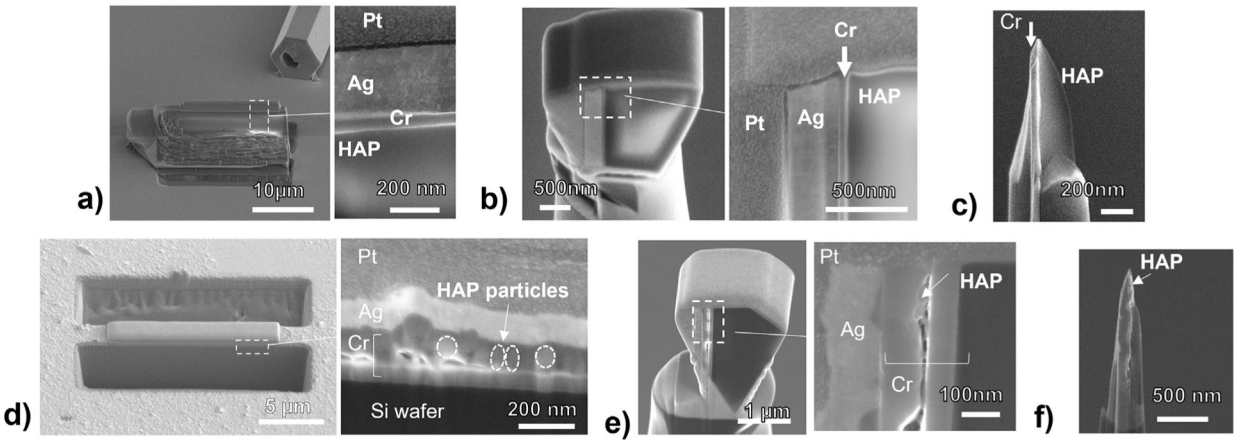

Fig. 2.

APT specimen preparation protocol for (a-c) protein-adsorbed and (d-f) amelogenin-mineralized HAP specimens by FIB-SEM. (a) Cross-sectional view showing the region on a protein-adsorbed specimen isolated for APT analyses and the layers of coatings deposited. (b) A section from the liftout mounted on a Si micropost after 90° rotation, showing the new orientation for the layered structure. (c) The final APT tip geometry for the protein-adsorbed specimen, capturing the protein-mineral interface along the tip length. (d) Cross-sectional view showing the amelogenin-mineralized HAP crystallites embedded between the Cr-coatings. (e) A section from the liftout mounted on a Si-micropost after 90° rotation. (f) The final APT tip geometry capturing the amelogenin-mineralized HAP crystallites along the tip length.

Author Manuscript Author Manuscript Author Manuscript Author Manuscript

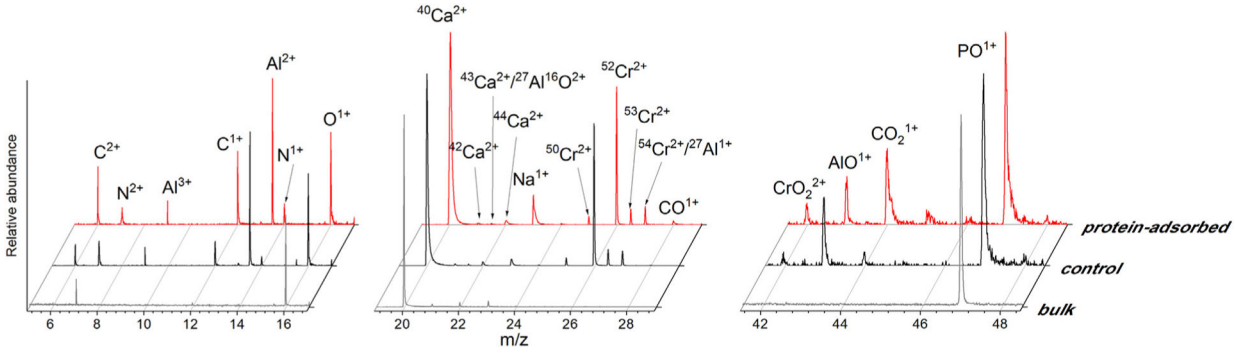

Fig. 3.

Mass spectral analyses. Comparison of APT *m*/*z* spectra for bulk HAP (gray), control (black), and protein-adsorbed (red) specimens within the ranges for the major elemental species of the HAP and Cr-coating and relevant organic species (C^{2+}, N^{2+}, C^{1+}, N^{1+}, CO^{1+}, and CO_2^{1+}). Each spectrum is normalized to the dominant species in the specified *m*/*z* range to better resolve individual peaks.

Author Manuscript Author Manuscript Author Manuscript Author Manuscript

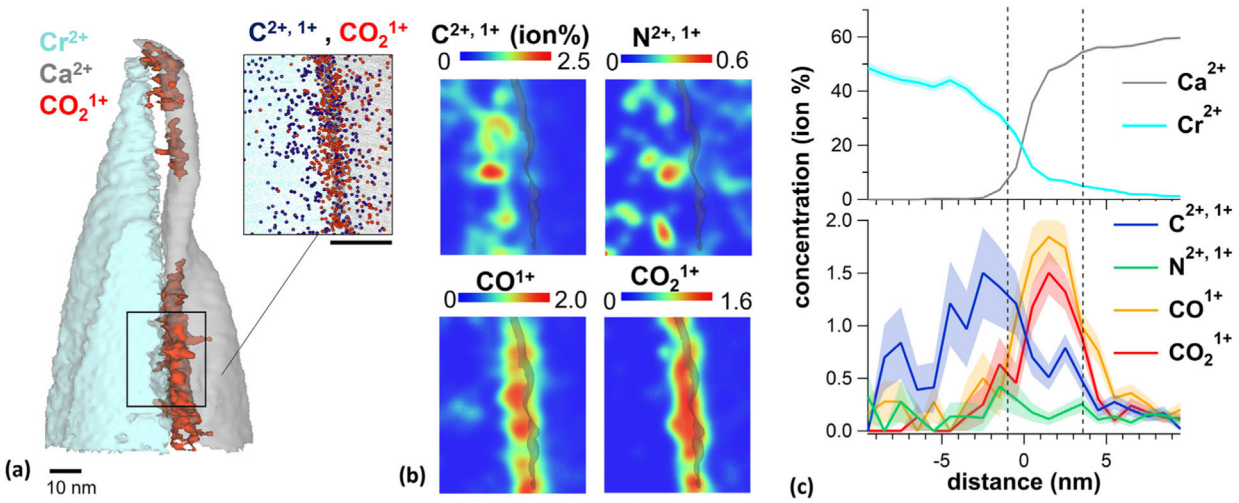

Fig. 4.

APT analyses of the protein-adsorbed specimen. (a) 3D chemical reconstruction showing the coating, HAP phase, and protein distribution, represented by isosurfaces of Cr (blue; 30 ion% Cr^{2+}), Ca (gray; 30 ion% Ca^{2+}), and CO_2 (red; 0.8 ion% CO_2^{1+}), respectively. The inset shows an atomic map highlighting the distribution of $C^{2+,\,1+}$ and CO_2^{1+} ions (blue and red ions, respectively) at the HAP surface (8 nm depth). (**b**) 2D concentration maps for the region in the panel (a) inset showing the distribution of organic species relative to the HAP surface (denoted by the gray line). (**c**) Concentration profiles showing the distribution of organic species (bottom graph) relative to the Cr-HAP interface (top graph). Dashed vertical lines mark the interfacial thickness for the HAP surface (i.e., 10%–90% relative Ca concentrations). The distance at 0 nm is relative to coating-HAP interface position (i.e., intersection of the Ca and Cr concentrations). Shading represents the expected error in concentrations.

Author Manuscript Author Manuscript Author Manuscript Author Manuscript

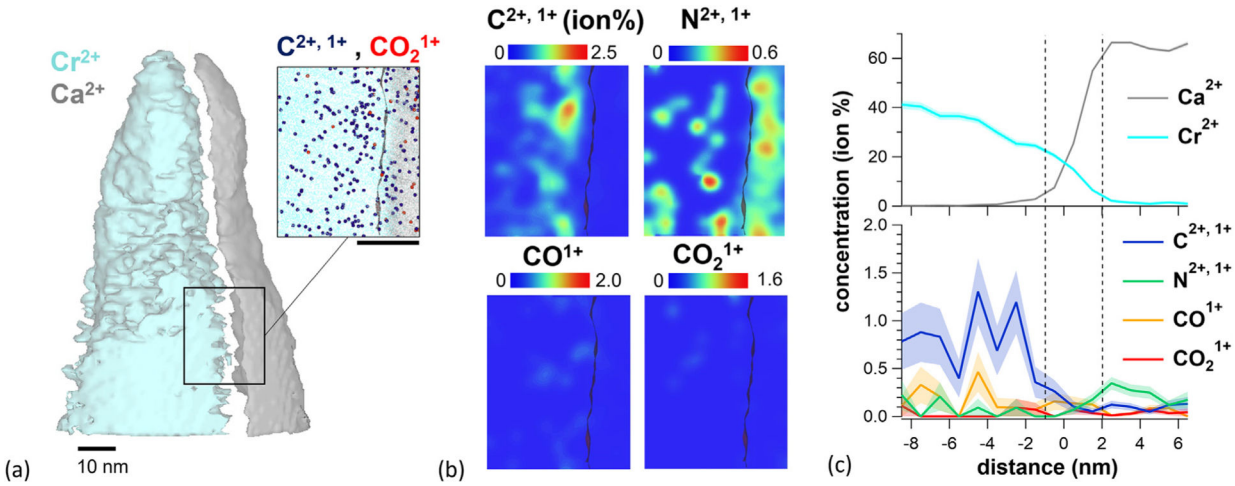

Fig. 5.

APT analyses of the control specimen. (a) 3D chemical reconstruction showing the coating and HAP phases, represented by Cr (blue; 30 ion% Cr^{1+}) and Ca isosurfaces (gray; 30% Ca^{2+}), respectively. Inset shows an atomic map highlighting the distribution of $C^{2+,\,1+}$ and CO_2^{1+} ions (blue and red ions, respectively) at the HAP surface (7 nm depth). (b) 2D concentration maps for the region in the panel (a) inset showing the distribution of organic species at the HAP surface (denoted by the gray line). (c) Concentration profiles showing the distribution of the organic species (bottom graph) relative to the Cr-HAP interface (top graph). The dashed vertical lines mark the interfacial thickness for the HAP surface (i.e., 10%–90% relative Ca concentrations). The distance at 0 nm is relative to the Cr-HAP interface position (i.e., intersection of the Ca and Cr ion concentration). Shading represents the expected error in concentrations.

Author Manuscript Author Manuscript Author Manuscript Author Manuscript

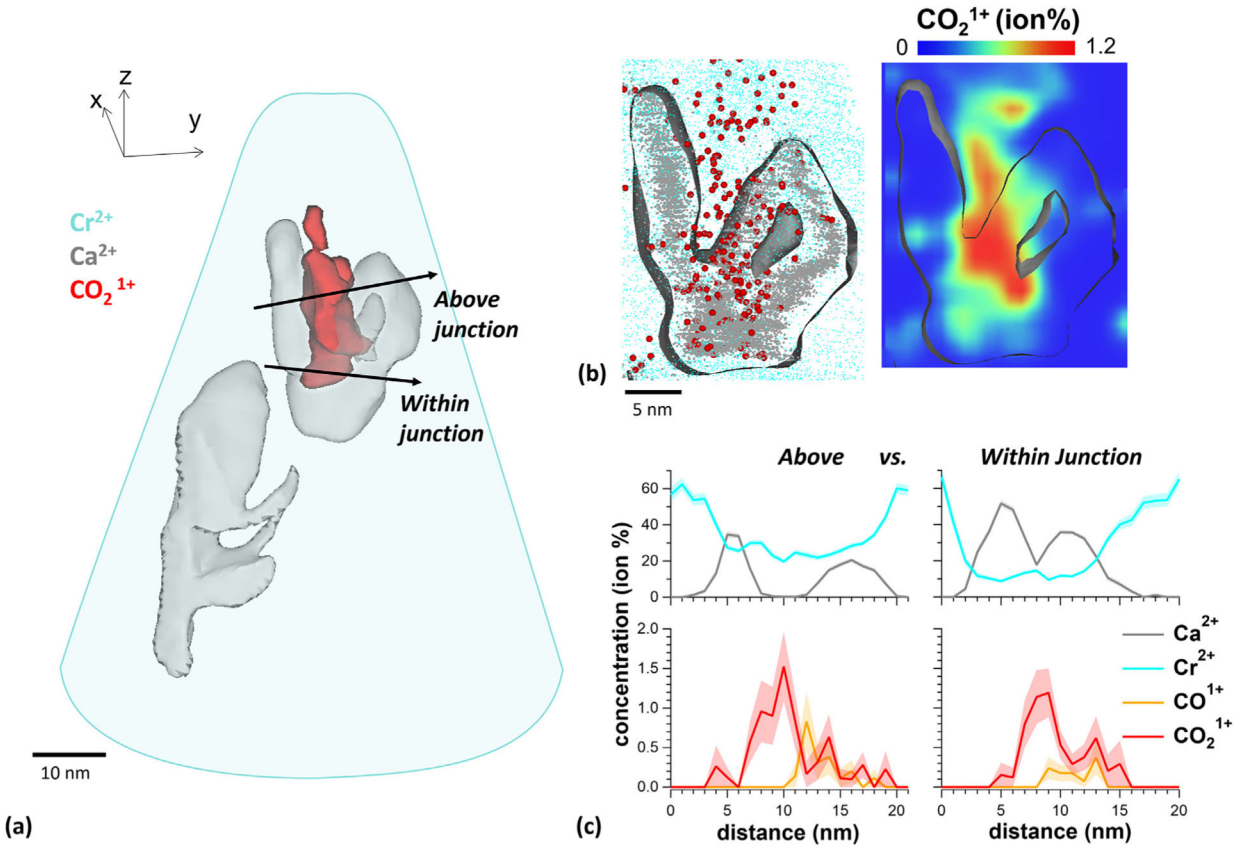

Fig. 6.

APT analyses of the amelogenin-mineralized HAP. (a) 3D chemical reconstruction showing HAP and amelogenin phases, represented by isosurfaces of Ca (gray; 8 ion%) and CO_2^{1+} (red; 0.8 ion%), respectively. The Cr-coating (blue) is outlined to allow clearer visualization of the protein-mineral interfacial structures. The Ca-rich, HAP particulate in the upper portion of the reconstruction is referred to as the "Y"-particulate while that below is the "F"-particulate. (b) Cross-section of the Y-particulate showing the atomic distribution (left) and correlative 2D concentration map (right) for CO_2^{1+} ions (red) relative to the HAP particulate (outlined by the gray isosurface). (c) Concentration profiles showing the distribution of the CO_x-species above vs. within the junction of the Y-particulate. Arrows in panel (a) denote the locations where the profiles were measured across. Shading represents the expected error in concentrations.

Author Manuscript Author Manuscript Author Manuscript Author Manuscript

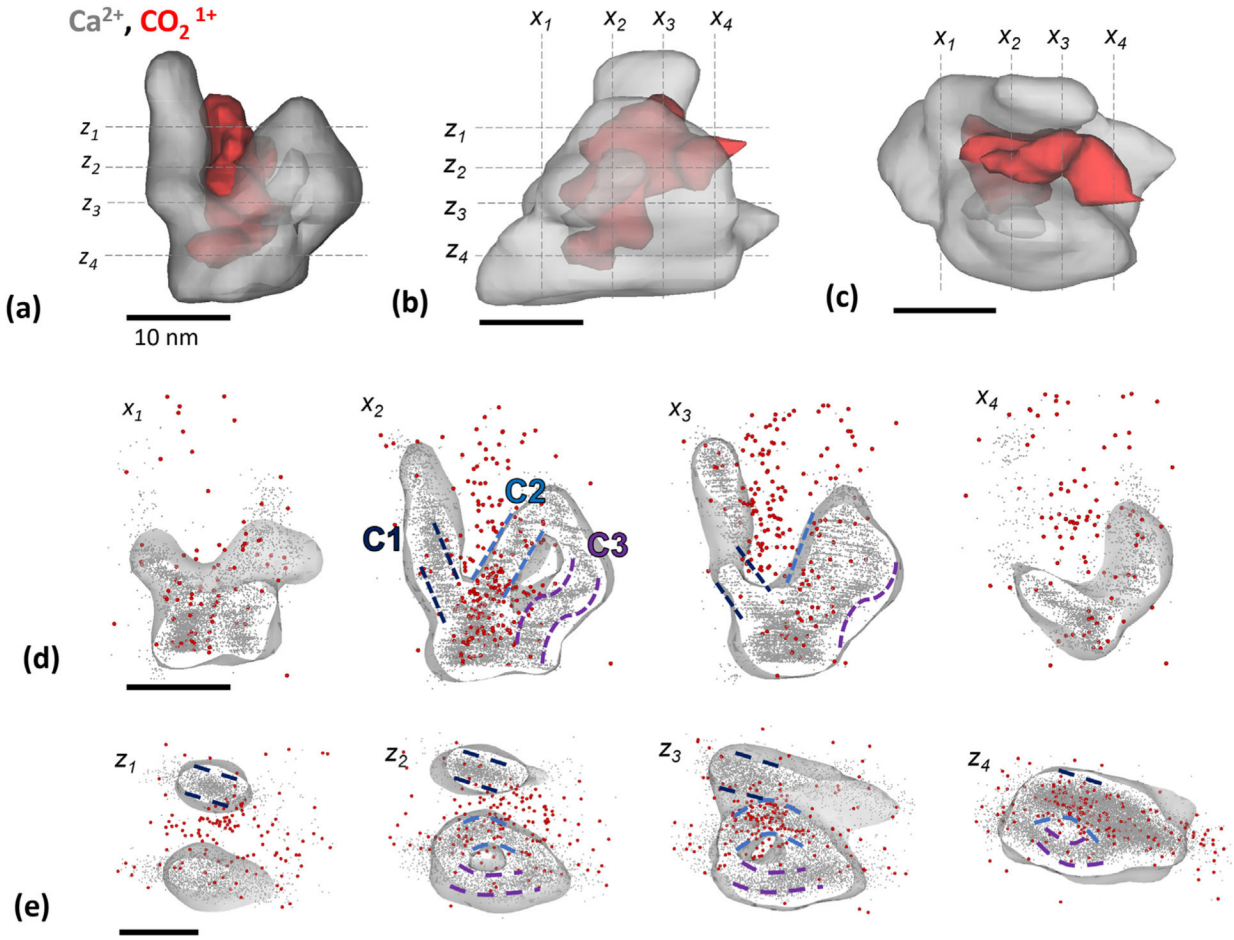

Fig. 7.

3D visualization and cross-sectional analyses of the Y-particulate in Fig. 6, looking down the (a) x-, (b) y-, and (c) z-directions. The HAP and protein morphologies are represented by Ca^{2+} (gray) and CO_2^{1+} (red) isosurfaces, respectively. Atomic maps representing cross-sections (3 nm depth) obtained along different depths of the particulate in the (d) x- and (e) z-directions, as marked in panels (aec). The general mineral particulate morphology is outlined in gray. Dashed lines of different colors denote individual HAP crystals labelled C1, C2, and C3, inferred from the spatial distribution of Ca^{2+} (gray) ions. The protein distribution is shown using CO_2^{1+} (red) ions.

Author Manuscript Author Manuscript Author Manuscript Author Manuscript

Table 1

Elemental and molecular ions identified in protein-adsorbed HAP MP.

Phase	Ionic species
HAP	O^{1+}, OH^{1+}, OH_2^{1+}, OH_3^{1+}, Ca^{2+}, Ca^{+1}, Cl^{1+}, PO^{1+}, PO_2^{1+}, PO_3^{1+}, P_2O^{2+}, P_2O^{1+}, PO_3^{1+}, P_xO_y (minor)
Cr-coating	Cr^{1+}, Cr^{2+}, Cr_2O^{2+}, CrO^{1+}, CrO^{2+}, CrO_2^{1+}, $CrOH^{1+}$, $CrOH^{3+}$, Al^{+1}, Al^{+2}, Al^{+3}, $Al_2O_2^{+3}$, $Al_2O_3^{+2}$, $Al_2OH_2^{+2}$, $AlNH^{+1}$, AlO^{+1}
Organics	C^{2+}, C^{1+}, CH^{1+}, CH_3^{1+}, CO^{1+}, CO_2^{1+}, N^{2+}, N^{1+}, NH^{1+}, NO^{1+}

Mater Today Adv. Author manuscript; available in PMC 2023 June 13.